Polymer 360 (2026) 130287

Contents lists available at ScienceDirect

Polymer

journal homepage: www.elsevier.com/locate/polymer

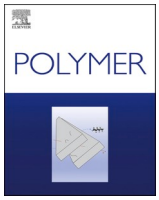

Spatial heterogeneity in polymer blends and its impact on dynamics

Bret W. Tantorno [a,1], Tuyen T.T. Truong [a,1], Lori M. Hoover [a], Gregory B. McKenna [a,*], Ran Tao [b], Fan Zhang [b]

[a] Department of Chemical and Biomolecular Engineering, North Carolina State University, Raleigh, NC, 27695-7905, USA
[b] Materials Measurement Science Division, Material Measurement Laboratory, National Institute of Standards and Technology, Gaithersburg, MD, 20899, USA

ARTICLE INFO

Keywords:
Polymer blend
PMMA
PEO
Dynamic heterogeneity
Miscibility
DSC
Rheology
WAXS
SAXS
USAXS

ABSTRACT

The relationship between dynamic and spatial heterogeneity in polymer blends is still not fully understood, yet it plays a crucial role in our understanding of their viscoelastic properties. Here, we report the results of an investigation of the viscoelastic response of a set of poly(ethylene oxide) (PEO)-poly(methyl methacrylate) (PMMA)-dimethylacetamide (DMAc) ternary blends, with emphasis on the nominally miscible regime. The work reveals interesting deviations from time-temperature superposition (TTS) as evidenced through van Gurp-Palmen (vGP) analysis. While previous rheological studies on such systems have focused on the terminal regime, our work extends through the Rouse- and towards the glassy-regime to broaden the range of dynamic behavior probed. We find that PEO:PMMA(DMAc) blends show thermal and rheological compatibility at PEO mass fractions below 30 % in the rubbery and terminal regimes. However, as the system dynamics go through the Rouse-regime and approach the glassy or α-relaxation (glass transition regime) the vGP plots no longer form a single curve, thus revealing a breakdown in TTS. These results both suggest that small-scale heterogeneities with distinct temperature dependencies exist, i.e., the blends are immiscible, and that the vGP plots are much more sensitive to breakdown of TTS than is the creation of the master curves themselves. Thus, it appears that the vGP analysis provides a sensitive measure of dynamic heterogeneity, highlighting subtle deviations that are not seen in standard TTS analysis. Additionally, in the system studied here, the ternary nature of the blends (PMMA-DMAc-PEO) includes a solvent and this alters the T_g and relaxation dynamics, and we describe how this impacts the reported outcomes. Our findings suggest that, as the polymer blends approach the α-relaxation, small-scale heterogeneities influence the dynamics such that they show different temperature dependencies, leading to dynamic heterogeneity. We also show results from wide-angle X-ray scattering (WAXS), small-angle X-ray scattering (SAXS), and ultra-small-angle X-ray scattering (USAXS) investigations that support the observations from the viscoelastic measurements.

1. Introduction

There is a growing body of evidence suggesting that subtle deviations from time-temperature superposition (TTS) or frequency-temperature superposition (FTS) in polymers can be more effectively analyzed using van Gurp-Palmen (vGP) plots than through traditional double-logarithmic representations of viscoelastic master curves [1–5]. By examining the phase angle (δ) as a function of the logarithm of the magnitude of the complex modulus ($|G^*|$), vGP analysis can potentially provide a sensitive means of identifying dynamic heterogeneity in complex fluids [5]. This approach offers a promising framework for identifying such heterogeneities and their relationship to underlying spatial heterogeneity in complex systems, including polymer blends and block copolymers, where the interplay of microstructure and dynamics is of fundamental interest.

Poly(ethylene oxide):poly(methyl methacrylate) (PEO:PMMA) blends have been extensively studied, with their thermodynamic miscibility well-documented in terms of composition and temperature. Above PEO's melting point, techniques such as differential scanning calorimetry (DSC), small-angle X-ray scattering (SAXS) [6–9], and small-angle neutron scattering (SANS) [10] demonstrate miscibility across the entire composition range. Below the melting point, however, PEO tends to phase separate and crystallize, with PMMA interfering with crystallization [11–13]. Conversely, complementary investigations

* Corresponding author.
E-mail address: gbmckenn@ncsu.edu (G.B. McKenna).
[1] These two authors made equal contributions to the work.

https://doi.org/10.1016/j.polymer.2026.130287
Received 7 February 2026; Received in revised form 16 May 2026; Accepted 24 May 2026
Available online 28 May 2026

using DSC, dielectric spectroscopy [14], density analysis [15], Fourier-transform infrared spectroscopy (FTIR) [16], and ^{13}C solid-state nuclear magnetic resonance (NMR) [17,18] reported no PEO phase separation and crystallization for blends containing less than 30 % mass fractions of PEO, below the melting point of PEO, suggesting that these blends are miscible at lower PEO concentrations. These studies were conducted on PEO:PMMA samples in which PEO crystallized, because the cooling process was not rapid enough to avoid crystallization. If the PEO phase separation and crystallization could be prevented, the blends might retain their miscibility, though this was not attempted.

The prior studies focused on the thermodynamic miscibility of the PEO:PMMA blends, while the dynamic compatibility (or heterogeneity) remains less explored. However, rheological studies, including those by van Gurp and Palmen [19], as well as Colby [20], have reported that PEO:PMMA blends do not follow TTS under miscible conditions, i.e., above the melting point of PEO. This incompatibility was attributed to the large difference in relaxation times between PEO and PMMA, and the conclusion has also been supported by infrared dichroism and birefringence studies performed simultaneously with dynamic studies conducted by Zawada et al. [21] Furthermore, prior studies have explored dynamic heterogeneity through the use of Cole-Cole plots [22], where a slight breakdown in TTS can be observed in the terminal regime. However, we contend that the vGP plot is superior for representing the broad range of dynamics investigated here where we examine the behavior from terminal to glassy relaxations. Due to the vast range of modulus magnitudes, the Cole-Cole type of analysis necessitates multiple "zoomed-in" subplots to capture the full breadth of the data, while the vGP plot provides a visualization of the entire range of data in one plot.

The apparent discrepancy between thermodynamic miscibility and the observation of dynamic heterogeneity under identical conditions, yet using different experimental techniques, may arise from nanoscale heterogeneities that are undetectable by conventional techniques like DSC but become evident in NMR experiments [17,18] that detect possible heterogeneity below a length scale of 20 nm. By leveraging vGP analysis to probe such possible subtle heterogeneities, we offer a new perspective on the miscibility of PEO:PMMA blends and the broader implications of polymer blend design. In the present study, DMAc was incorporated into the PMMA phase to lower the glass transition temperature of neat PMMA closer to that of PEO, thereby preventing potential PEO degradation in the terminal regime, as shown subsequently. The present work uses the ternary PEO:PMMA(DMAc) blend to broaden the range of dynamics investigated. In the prior work on binary PEO:PMMA blends, the studies focused on the terminal behavior. The current work extends the prior studies by examining both the full range of dynamics from terminal, to rubbery, to Rouse, and towards the glassy (or α-relaxation) regimes, thus providing insights into our understanding of the interplay between microstructure and viscoelastic dynamics. These ternary blends exhibit apparent TTS compatibility in their dynamics, unlike the prior work on binary PEO:PMMA blends which show TTS breakdown. However, they also show anomalous behavior in the corresponding vGP plots. Specifically, deviations in the phase angle from expected trends suggest the presence of nanoscale dynamic heterogeneities. Such anomalies provide an alternative route to characterizing blend miscibility and homogeneity, with implications for understanding and tuning the properties of polymer blends. It also provides insights related to conventional frequency-temperature superposition analysis. In addition to the blend rheology, we also employed synchrotron-based WAXS and SAXS measurements to examine a subset of the nominally compatible blends and these results further support our conclusions.

2. Experimental methods

2.1. Sample preparation

Polyethylene oxide (PEO, $M_w = 125{,}000$ g/mol, PDI = 1.88), poly (methyl methacrylate) (PMMA, $M_w = 100{,}000$ g/mol, PDI = 1.33), and dimethylacetamide (DMAc) were purchased from Thermo Fisher Scientific Inc.[2] The molecular weight and polydispersity index (PDI) were determined by gel permeation chromatography (GPC) from Resolve-Mass Laboratories Inc. (Supplemental Information). Polymer blend plaques of PEO:PMMA(DMAc) were prepared by a solvent casting procedure as shown in Fig. 1. First, the polymers were dissolved in DMAc by continuous stirring at 50 °C for 24 h. Then, the pure polymer solutions of PEO and PMMA were mixed at the appropriate ratios to produce mixtures of 0 % to 100 % mass fractions of PEO to PMMA in 10 % mass fraction increments. An additional plaque of PEO at a mass fraction of 5 % was made as well. The PEO:PMMA(DMAc) blends with varying mass fractions are denoted as PEO:PMMA(DMAc) for simplicity, representing the mass fraction ratios of PEO to PMMA that were mixed. The actual compositions of the ternary blends are given in Table 1. The mixtures were then stirred for an additional 24 h at 50 °C to ensure uniform mixing. After mixing, the solutions were poured onto a Teflon evaporation disk and transferred to a 60 °C oven for 2 days to dry. Similar treatments were applied to the pure PMMA and PEO materials to understand the impact of solvent on the results. The as-cast plaques had thicknesses of approximately 750 μm and were cut out with an 8 mm hole punch. Also, neat PMMA and neat PEO as received were used without solvent treatment for comparison. The neat PMMA and neat PEO samples were press-molded in an 8 mm mold at 115 °C and 65 °C, respectively, to a final thickness of about 1 mm.

2.2. Rheological measurements

Dynamic oscillatory measurements were conducted using a TA Instruments AR-G2 controlled-stress rheometer with an 8 mm parallel plate geometry. All measurements were performed in the strain-controlled mode using the manufacturer's software for strain-control on the stress-controlled rheometer. Three identical samples were prepared and tested from each of the same solvent-cast plaque to ensure reproducibility. An example can be found in the Supplemental Information (SI; Fig. S5). Compliance corrections were applied to the data before further analysis [23,24]. Neat PMMA and PEO were thermally molded from manufacturer-provided powders in an 8 mm diameter mold, 1 mm thick, to serve as a reference for the solvent-cast plaques. The temperature range for testing of the neat PMMA was 120 °C to 200 °C, while neat PEO was tested from 60 °C to 120 °C since PEO crystallizes below 60 °C. For the solvent-cast plaques, 8 mm disc-shaped samples were created using an 8 mm diameter punch. As described subsequently, the plasticizer content of the PMMA produced from the casting procedure was approximately 11%. The temperature range for the PMMA(DMAc) and PEO plaques was 60 °C to 140 °C and 60 °C to 120 °C, respectively. The temperature range for the PEO:PMMA(DMAc) plaque blends was 50 °C to 140 °C, except for the blend with 5 % mass fraction of PEO, which was 60 °C to 140 °C. The dynamic frequency sweeps were performed over a frequency range of 0.1 rad/s to 100 rad/s at a strain of 1 % for the terminal regime, and adjusted to 0.05 % for the glassy regime, for all samples.

For the oscillatory temperature sweep measurements, a strain-controlled rheometer, Advanced Rheometric Expansion System (ARES), equipped with a 2KFRT transducer and liquid nitrogen for cooling, was used with the rectangular torsion fixtures. Neat PMMA, obtained from the manufacturer, was press-molded into a rectangular shape and the solvent-cast PMMA(DMAc) (plaque) was cut into a rectangle, both with dimensions of approximately (24.90 × 12.6 × 1.2) mm.

[2] Certain commercial products, commercial and open source software are identified in this paper to specify the materials used and the procedures employed. In no case does such identification imply endorsement or recommendation by the National Institute of Standards and Technology, nor does it indicate that the products are necessarily the best available for the purpose.

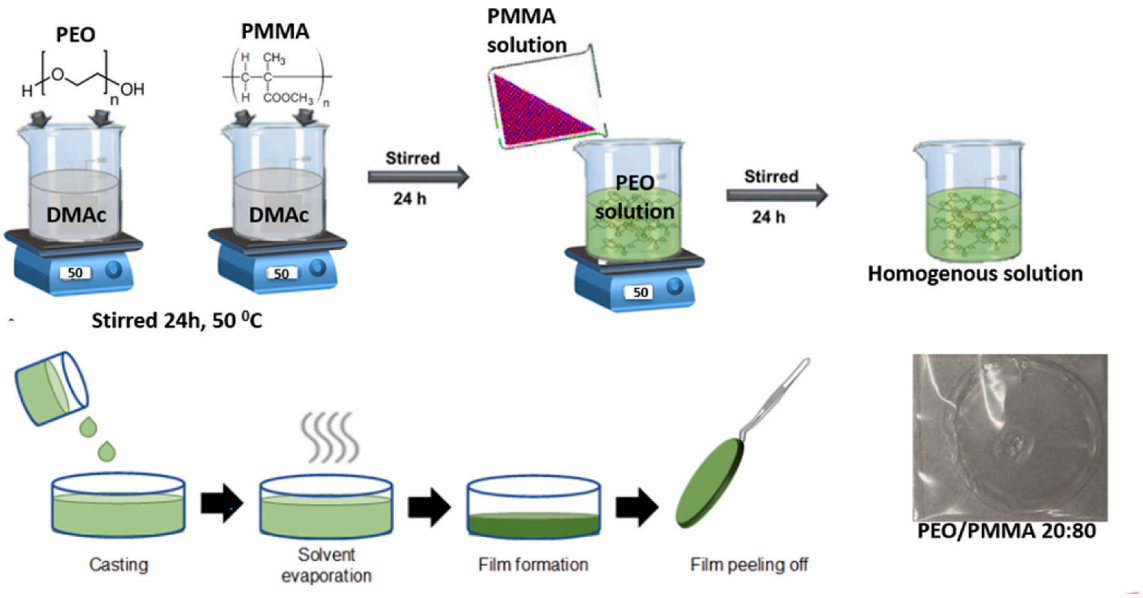

Fig. 1. PEO:PMMA(DMAc) blend plaque preparation process.

Table 1
Compositions of the as-cast plaque samples.

Sample	% mass fraction PEO	% mass fraction PMMA	% mass fraction DMAc
0:100	0	89	11
5:95	4	85	11
10:90	9	81	10
20:80	18	73	9
30:70	28	64	8
40:60	37	56	7
50:50	47	47	6
60:40	57	38	5
70:30	67	29	4
80:20	78	20	2
90:10	89	10	1
100:0	100	0	0

Temperature sweeps at a heating rate of 2 °C/min were performed from (−50 to 75) °C for the PMMA(DMAc) plaque made by solvent casting and from (−50 to 135) °C for the neat PMMA. The test was conducted at a strain of 0.05 % with a frequency of 1 rad/s.

2.3. Differential scanning calorimetry

Differential scanning calorimetry (DSC) was carried out using a Mettler Toledo DSC823e system equipped with a Freon intercooler under a nitrogen purge. The instrument was calibrated for temperature and heat flow before each run using the melting point of indium, employing a heating rate of 10 °C/min. Samples prepared from the solvent-cast plaques were cut to size with a razor blade, while neat PMMA and PEO sample powders were placed directly into the DSC pans. Sample masses were 10.00 ± 0.46 mg and the calorimetry scans for each sample were run three times to ensure reproducibility. Initially, a heating rate of 10 °C/min was applied from ambient temperature, followed by an isothermal hold at 150 °C for 1 min to remove any prior thermal history in the material. Subsequently, a cooling step at 10 °C/min was executed to −70 °C. After completing the cooling scan, a second heating run was performed at a rate of 30 °C/min, from −70 °C to 150 °C, to determine the apparent melting temperature (T_m), melting enthalpy (ΔH_m), and glass transition temperature (T_g). Then, a second cooling and heating sequence with the same rates and temperature range was performed to ensure result reproducibility. The T_g was obtained using the limiting fictive temperature as determined by applying the Moynihan area matching method [25] to the heating data. The average and standard deviations of the measurements are given in Table S1. Also, each sample was weighed before and after the experiment to determine the weight loss attributed to residual solvent, moisture, and/or degradation. These aspects are further discussed subsequently.

2.4. Thermogravimetric analysis

Thermogravimetric analysis (TGA) was conducted using a Mettler Toledo TGA 2 equipped with a Freon® intercooler and nitrogen purge gas. Isothermal experiments at 175 °C and 140 °C were performed for 4 h and 1 h, respectively, on samples cut from the polymer plaques, each weighing approximately (17.5 ± 2.2) mg. The resulting data was used to determine the concentration of DMAc in the plaques after the solvent-casting process.

2.5. Wide-angle X-ray scattering and small-angle X-ray scattering measurements

Synchrotron-based wide-angle (WAXS), small-angle (SAXS), and ultra-small-angle (USAXS) X-ray scattering experiments were performed at the Advanced Photon Source, Argonne National Laboratory in the USAXS facility on beamline 12-ID-E. All measurements were conducted using 28 keV X-rays, providing a continuous q range from approximately 0.0001 $Å^{-1}$ to 6 $Å^{-1}$, with a beam size of 0.8 mm × 0.8 mm. The instrument employs Bonse-Hart optics for angular collimation and analysis, utilizing two CdTe detectors: an Eiger 1 M for WAXS and a Pilatus 100K for SAXS. More details about this instrument can be found elsewhere [26].

3. Results and discussion

3.1. Characterization of the solvent in the PEO and PMMA plaques

To prepare the ternary blends, the solvent casting procedure described above was used. To quantify the solvent content in the PMMA and PEO phases, thermogravimetric analysis (TGA) was performed on both the neat polymers and the solvent-cast plaques from DMAc. The PEO and PMMA were prepared in the same procedure as the PEO:PMMA (DMAc) blends by solvent casting from the DMAc as described in the Sample Preparation section above. Fig. 2(a) shows how the mass of the

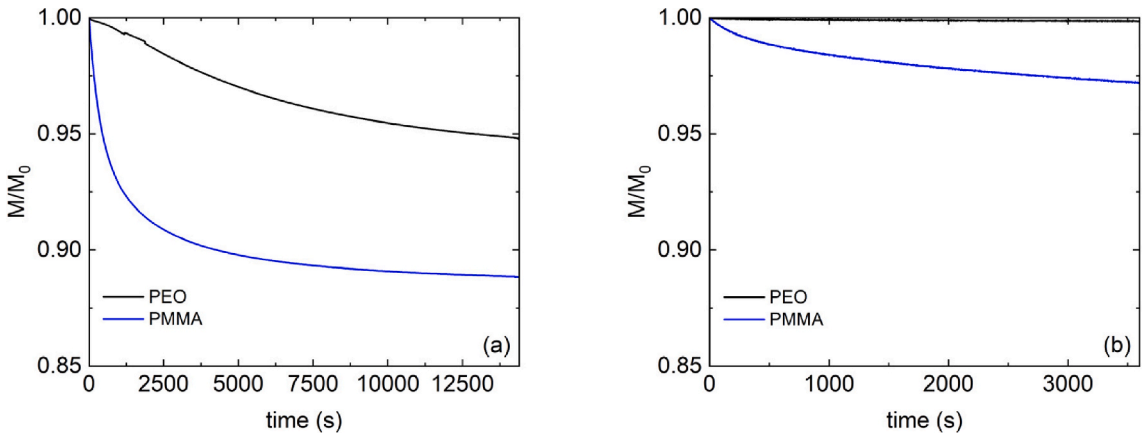

Fig. 2. Normalized mass (M/M_0) of the solvent-cast PEO and PMMA(DMAc) 10 °C above the boiling point of DMAc at 175 °C (a) and at the highest experimental temperature during rheometry at 140 °C (b) measured by TGA.

samples evolves over 4 h during an isothermal hold at 175 °C, which is 10 °C above the boiling point of DMAc. Even after an hour at 10 °C above the boiling point, the samples continue to lose mass at a slow rate. After 4 h, the PEO and PMMA lost 3.1 % and 11.2 % of their mass, respectively. The quantity of DMAc remaining in the PMMA plaques suggests that PMMA forms hydrogen bonds with DMAc, a phenomenon previously documented in the literature showing that PMMA can hydrogen bond with solvents [27] such as DMAc. Consequently, the solvent-cast PMMA plaque will be denoted as PMMA(DMAc) to emphasize that this phase has properties distinct from those of neat PMMA. Additionally, the 3.1 % mass loss in PEO is attributed to thermal degradation rather than solvent evaporation, as evidenced by a consistent glass transition temperature and rheological properties (in the temperature range studied) between neat PEO and the PEO plaque, along with a characteristic color change indicative of degradation for the TGA sample of PEO.

Fig. 2(b) shows the results of the TGA experiments performed at the highest rheological experimental temperature of 140 °C for an hour. Under these conditions, the PEO and PMMA(DMAc) lost 0.2 % and 2.8 % of their mass, respectively. Most of the DMAc escapes from the samples during the first 15 min. Given that a single frequency sweep experiment at one temperature lasted approximately 9.5 min, we estimate that the PEO and PMMA(DMAc) would lose approximately 0.07 % and 1.2 % of their mass at this temperature, respectively. Note that the mass loss in the PEO is attributed to degradation rather than solvent loss.

Additionally, in the TGA experiments, the samples are exposed to a surrounding nitrogen atmosphere, allowing DMAc diffusion from all dimensions. In contrast, during the rheological experiments, DMAc can only diffuse out through the edges of the 8 mm plates that have a gap or plaque thickness of approximately 750 μm. This suggests that DMAc loss during rheological experiments would be substantially lower than in the TGA experiments due to these diffusion constraints. Notably, no bubbles formed in the plaques during or after the rheological experiments, indicating minimal solvent loss.

Since the PEO plaque showed signs of degradation but no evidence of solvent loss, the PMMA(DMAc) plaque was selected to study solvent stability during rheological testing. The PMMA(DMAc) plaque was cycled from 140 °C to 50 °C and then back to 140 °C to examine rheological changes associated with solvent loss. Since the frequency (ω) sweeps were conducted from high to low temperatures, starting at 140 °C and decreasing to 50 °C, it is reasonable to assume that the majority of DMAc evaporated at 140 °C, with minimal loss at lower temperatures. This is supported by the data shown in Fig. 3. Fig. 3(a) presents the results from the 140 °C experiments, and Fig. 3(b) shows those from the 100 °C experiments. The tests were conducted sequentially. While a shift in the data is observed at 140 °C, little to no change occurred at 100 °C, indicating negligible DMAc loss at the lower temperatures (The SI shows the 110 °C, 120 °C, and 130 °C scans in Fig. S6). Comparing the 140 °C experiments at 0.1 rad/s, where the data shift is most pronounced, reveals a 0.42-decade difference between the first and second runs in storage modulus G'. Assuming that there is approximately a 3 °C change in T_g per decade of frequency [28], this corresponds to an

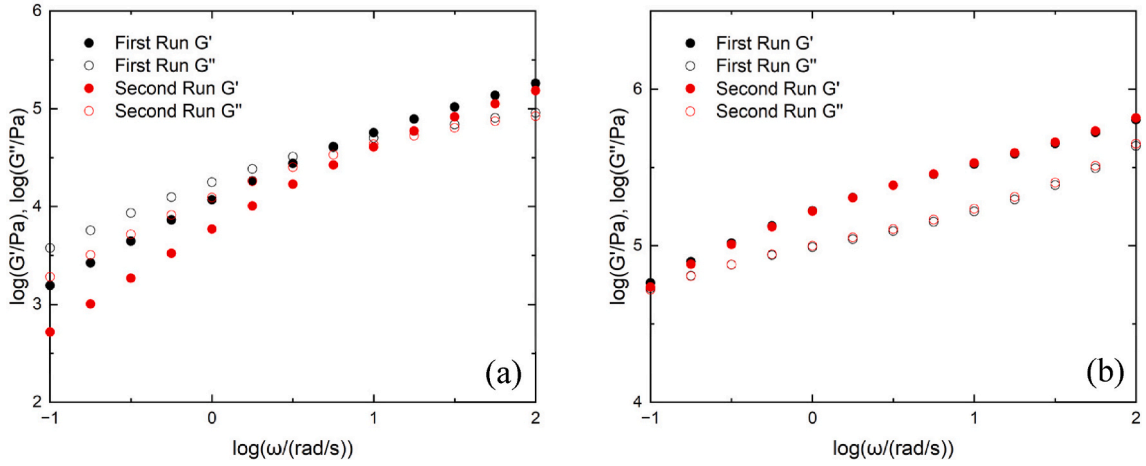

Fig. 3. Rheological experiments on the PMMA(DMAc) plaque at 140 °C (a) and 100 °C (b). Here, G′, G″, and ω are storage modulus, loss modulus, and angular frequency, respectively.

estimated 1.3 °C shift in T_g, suggesting a slight alteration in the material properties at the higher temperatures. Importantly, at the lower temperatures, the material composition remains stable.

Understanding how the solvent influences the PMMA(DMAc) plaque is important at lower temperatures, since the blend remains stable. To examine this issue, we carried out temperature scans on the pure PMMA and on the PMMA(DMAc). The samples were placed in the rheometer and cooled to −50 °C and reheated at 2 °C/min. As seen in Fig. 4 as a plot of the tangent of the phase angle (δ) vs. T, the solvent has a clear effect in decreasing the T_g of PMMA, shifting the relaxation dynamics closer to those of PEO (where $T_g = -50.5$ °C). In addition, the β-relaxation of the PMMA also shifts downwards in temperature. While there is a clear decrease in T_g from 109.9 °C to 57.8 °C and a decrease in the β-relaxation from 2.5 °C to −8.6 °C (Fig. 4 inset), the magnitude of the decrease in the β-relaxation is not as large as the decrease in the T_g or α-relaxation, thus increasing the likelihood of overlap between the two mechanisms. Since the relaxation dynamics of PMMA are shifted closer to those of PEO, the rheological response of the PEO:PMMA(DMAc) is expected to be different from the PEO:PMMA blend. Here, we examine a PEO:PMMA(DMAc) ternary blend, in which the dynamic behavior of the PMMA phase has been altered closer to that of PEO. This distinction is particularly important when comparing our rheological data to values reported in the literature and when interpreting our own results in the following sections.

3.2. Comparisons with literature data for PEO:PMMA blends

In the following discussion, we compare the present rheological results with those from previous studies of the time-temperature superposition (TTS) behavior of PEO:PMMA binary blends. For example, Colby [20] carried out oscillatory shear experiments on a mass fraction of 20.2 % PEO (235,000 g/mol) in PMMA (107,000 g/mol) sample at (120, 137, 155, and 174) °C, i.e., well above the melting point of PEO and at a composition where the blend is thought to be miscible. Their data, digitized from the original publication, are shown in Fig. 5(a), and we see that despite the nominal miscibility at these temperatures, there is a clear breakdown of TTS. He attributed the breakdown to the PMMA and PEO within the blends sensing the local environment differently, i.e,

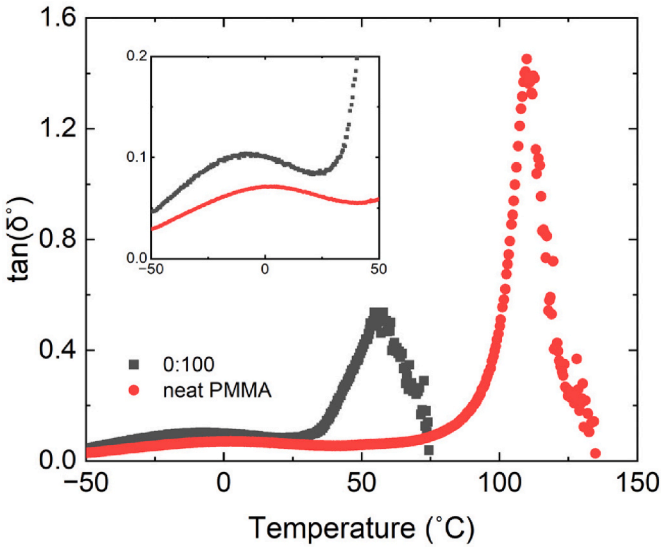

Fig. 4. The relaxation dynamics for the PMMA(DMAc) plaque in black squares and PMMA from the manufacturer in red circles. Experiments were conducted at a heating rate of 2 °C/min with 0.05% strain and 1 rad/s. The inset shows an enlarged view of the β-relaxation range. (For interpretation of the references to color in this figure legend, the reader is referred to the Web version of this article.)

the polymer chain sees a heterogeneous environment with other chains, leading to different temperature dependences of the global dynamics.

However, it is worth noting that the work by Colby may have had issues due to residual solvent or how he treated the samples to remove the solvent. In that work, he used acetone as the co-solvent in the blend preparation, whereas in the present work, we used DMAc. Acetone has a significantly lower boiling point than DMAc (viz., $T_{b,\ acetone} = 56.2$ °C; $T_{b,\ DMAc} = 165$ °C) [29], but it also remains in the PMMA. To address this, Colby employed an extensive sample preparation process. After drying the samples for three weeks near the relevant T_g, the samples were then molded 50 °C above T_g or T_m, followed by heating the samples above 174 °C under nitrogen to boil off the remaining solvent. The process was repeated until no bubbles formed during the experiment. It is our thought that this extensive, though meticulous, preparation could have led to the degradation of the PEO, and this would account for some discrepancies in the superimposing of the curves or differences from the present study. As a reminder, our TGA experiments showed that PEO undergoes thermal degradation at 175 °C and lost approximately 2 % of its mass after 4 h under a nitrogen atmosphere. The timescales for the Colby sample treatment subsequent to the three-week drying at 50 °C were not reported. Regardless, Colby's data show significant differences from our data and clearly do not follow TTS.

In another study, Van Gurp and Palmen [19] investigated the dynamics of a PEO:PMMA blend (molecular weights not given) with a mass fraction of 35 % PEO at temperatures of (70, 90, 110, 130, 150, 170, 190, and 210) °C, as shown in Fig. 5(b). The results were similar to those of Colby in that the curves did not superimpose; however, the curves had dissimilar behavior. As seen in Fig. 5(a), the breakdown in superposability was of a different character. The G′(ω) data seem superposed while the G" (ω) data seem to fall off of a master curve in a way that is reminiscent of a β-relaxation [30–32]. Van-Gurp and Palmen attributed the breakdown in TTS to local frictional force interactions within the material. The local frictional force interactions refer to the forces between adjacent polymer segments that move relative to one another. For instance, the different forces between PMMA and PEO dominant segments, a spatial heterogeneity, lead to the dynamic heterogeneity response in the blend's behavior. Despite their experiments being performed on an immiscible composition, the blend should have been miscible at the elevated temperatures, above PEO's melting point, and have been superimposable. It is interesting that both Colby and van Gurp and Palmen performed experiments on compositions at temperatures where they should be miscible according to DSC, but found a clear breakdown in TTS. It is also of interest that the terminal flow regimes and the roll-off from the rubbery plateau seem to superimpose, while the response going towards the Rouse regime seems to exhibit the non-superposing response.

One explanation may be a strong molecular weight effect between the different molecular weights of PEO in this study (125,000 g/mol), Colby's (235,000 g/mol), and perhaps van Gurp and Palmen's (given the higher rubbery plateau seen in their data). Another explanation for why our loss modulus superimposes, while Colby's and van Gurp and Palmen's do not, is the effect of the solvent in our samples. As noted earlier, the α- and β-relaxations of PMMA are shifted to lower temperatures, bringing them closer to the relaxation mechanisms of PEO. It is also important to note that the Colby and the van Gurp and Palmen data only cover the terminal to rubbery regimes, but do not extend into the Rouse towards the glassy regime. To further investigate these differences, both the phase behavior and rheological response are examined in the following sections.

3.3. Phase diagram behavior

The phase diagram of the PEO:PMMA(DMAc) was determined from DSC measurements, and the results are presented in Fig. 6. (The SI shows a plot of the DSC heating traces in Fig. S1). The samples exhibit a single T_g from (0 to 20) % mass fraction of PEO, indicating miscibility within

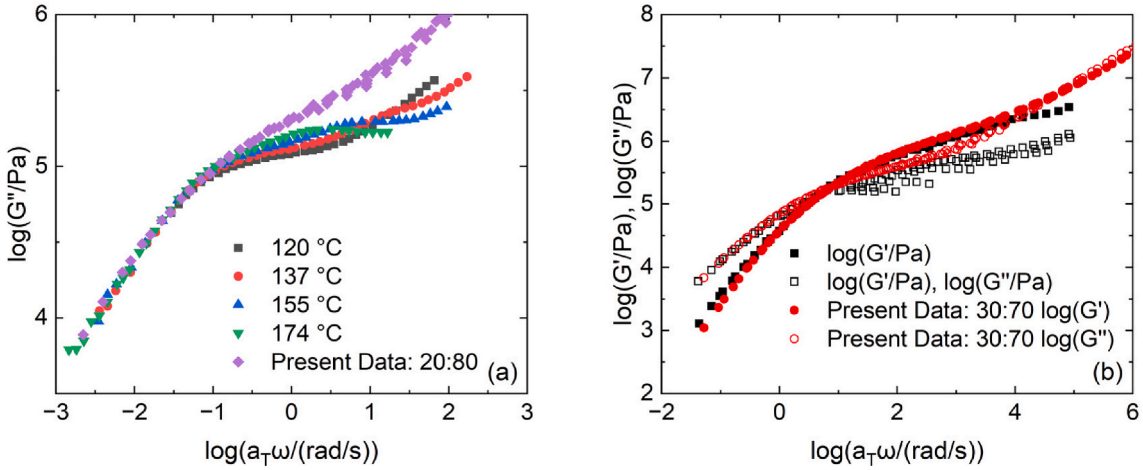

Fig. 5. Comparisons between the present data and data. Colby's (a) data of PEO:PMMA blends with a mass fraction 20.2 % PEO [20] in black, red, blue, and green compared with our data with mass fraction of 20 % PEO in magenta. Van Gurp and Palmen's (b) data with mass fraction of 35 % PEO [19] in black compared with our data with mass fraction of 30 % PEO in red. (For interpretation of the references to color in this figure legend, the reader is referred to the Web version of this article.)

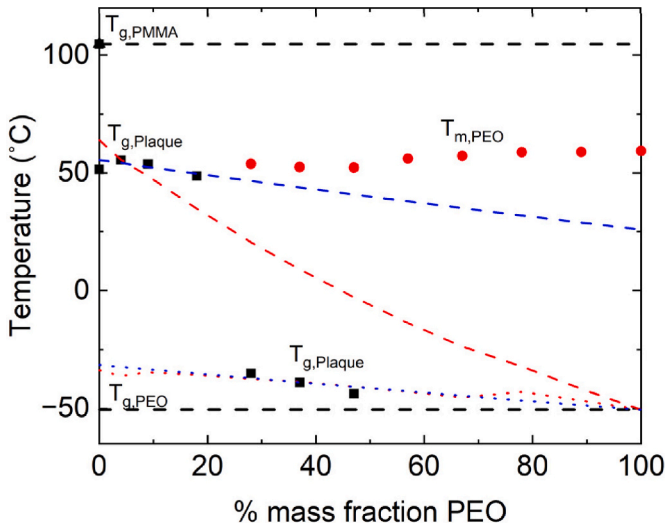

Fig. 6. Phase diagram for the PEO:PMMA(DMAc) plaques. Top and bottom dashed lines represent the pure T_g of PMMA and PEO, respectively. Black triangles represent the T_g of neat PMMA; black squares are the T_g values of the material containing DMAc solvent; red circles are the measured melting points of the PEO. The dashed red and blue lines represent the three-component Gordon-Taylor equation and the Lodge-McLeish model for the higher T_g values. The dotted red and blue lines represent the three-component Gordon-Taylor equation and the Lodge-McLeish model for the lower T_g values. (For interpretation of the references to color in this figure legend, the reader is referred to the Web version of this article.)

this composition range, based on the assumption that a single endothermic feature (i.e., a step change in heat capacity) is the signature of miscibility. An additional point to note is that the PMMA(DMAc) that did not contain any PEO has a T_g of 51.5 °C, which is significantly lower than neat PMMA from the manufacture. This deviation is due to the DMAc solvent retained during processing, which remains in the PMMA phase but not in the PEO. As discussed in the previous sections, the blends here are actually ternary blends where DMAc shifts the relaxation mechanism of PMMA into the normal melting range of PEO as well as closer to the PEO glass transition. At a mass fraction of 30 % PEO, a distinct T_g value is observed at −35.2 °C, while a small endothermic peak corresponding to melting is observed at 53.8 °C, indicating phase separation and immiscibility. The small endothermic peak in the 30 % mass fraction PEO plaque seems to interfere with the PMMA(DMAc) T_g, causing deviations in the baseline. As the PEO content increases beyond 30 % mass fraction of PEO, the melting of the PEO is observed more clearly, and this obstructs the T_g region of the dominant PMMA(DMAc) phase, confirming the mixture incompatibility at higher PEO content below the melting point of PEO. Notably, the lower T_g value observed in the (30, 40, and 50) % mass fraction of PEO plaques gradually decreases toward the T_g of pure PEO, at approximately −50.5 °C, which agrees with the literature [33]. For higher PEO compositions (60 % to 100 % mass fraction), no T_g was recorded because the DSC instrument had a low-temperature limit of (−75.0 °C) which is not sufficient to detect the full glassy line below the T_g of the phase-separated PEO. In conclusion, the blends are miscible at PEO mass fractions between 0 % and 20 %, and immiscible at PEO mass fractions from 30 % to 90 % below the melting point of PEO according to DSC. These findings are consistent with previously reported literature [14,15,17].

A key point of discussion regarding the 30 % mass fraction of PEO plaque is whether there are two glass transition temperatures. Due to the distortion of the baseline in the DSC heat flow curves due to the T_g and melting endotherms obstructing one another, it is possible that there are two T_gs, a dominant PMMA(DMAc) phase, and a dominant PEO phase. In our work, we attributed the second endothermic peak to PEO melting; however, in the work by Lodge et al. [34], two T_gs were reported for this composition, and they questioned if this necessarily indicates immiscibility. In their work, they applied the Lodge-McLeish model [35], Equations (1) and (2), to a PEO:PMMA blend, and their results suggested that miscible polymer blends can exhibit two T_g values. They attributed this to the local environments becoming enriched with the same species due to chain connectivity, resulting in relaxation times, or T_g's, that reflect the inherent mobilities of the individual components. However, this interpretation has been questioned by Zheng and Simon [36], who proposed that the model parameters might instead represent local concentration variations or interactions between the components, i.e., immiscibility.

$$\varphi_{eff} \stackrel{\text{def}}{=} \varphi_s + (1 - \varphi_s) \tag{1}$$

$$\frac{1}{T_g(\varphi_{eff})} = \frac{\varphi_{eff}}{T_{g,1}} + \frac{1 - \varphi_{eff}}{T_{g,2}} \tag{2}$$

It is also important to mention that Lodge et al. [34] used low molecular weight PEO (300 g/mol) and PMMA (10,000 g/mol) to mitigate PEO crystallization in the blends. This aspect of the study, raised by Zheng and Simon, suggests that the low molecular weight PEO may behave more like a solvent, where the self-concentration effect, which has an effective length-scale of approximately the Kuhn length cubed, is

small and this leads to the possibility that the model accounts for more than just chain connectivity. Overall, the phase diagram data from Lodge et al. are consistent with our results, except that in our system, the higher molecular weight PEO crystallizes at lower concentrations, and we do not observe two T_gs. The debate over whether the two T_g signatures result from the heterogeneities from concentration fluctuations or chain connectivity remains unresolved. For the remainder of the present discussion, we will explore the DSC response of supposedly miscible blends and for the 30 % PEO mass fraction plaque.

Fitting the Lodge-McLeish model (Equations (1) and (2)), where ϕ_s is the self-concentration, ϕ_{eff} is the effective-concentration, $T_g(\phi_{eff})$ is the glass transition of the mixture, and $T_{g,i}$ is the glass transition of component i, provides a good approximation of the upper and lower T_g values. The self-concentration of PEO and PMMA(DMAc) obtained from our data are 0.75 and 0.79, respectively, which are larger than those reported by Lodge et al. [34] ($\phi_{eff,PEO} = 0.55$ and $\phi_{eff,PMMA} = 0.60$). The main differences between our blends and theirs are the presence of having a matrix of PMMA(DMAc) rather than a pure PMMA phase and the large disparity in molecular weights. Despite our self-concentration values being larger, they remain on the order of the Kuhn length, which Lodge et al. suggest is the expected scale for self-concentration.

Another widely used model for predicting the glass transition is the Gordon-Taylor (GT) equation [37]. Because DMAc is present in the polymer blend, a three-component GT equation was applied, as shown in Equation (3). In this expression, T_g represents the glass transition of the mixture, k_{ij} represents the ratio of the heat capacity jump between component i and j ($k_{ij} = \frac{\Delta C_{pj}}{\Delta C_{pi}}$), and T_{gi} and w_i correspond to the glass transition and weight fraction of the pure components, respectively. PEO, PMMA, and DMAc were designated as components 1, 2, and 3, respectively. The T_g for DMAc was estimated at two-thirds of its melting point [38,39], approximately −104.4 °C. Fig. 6 shows the three-component GT model predictions for the upper and lower T_g values.

$$T_g = \frac{w_1 T_{g,1} + k_{12} w_2 T_{g,2} + k_{13} w_3 T_{g,3}}{w_1 + k_{12} w_2 + k_{13} w_3} \quad (3)$$

The $k_{PEO,\ PMMA}$ value was determined from the heat capacity jump between the glassy to liquid states and was calculated to be 0.58. In contrast, the $k_{PEO,\ DMAc}$ could not be obtained directly and was therefore treated as a fitting parameter. For the upper and lower T_g values, the corresponding $k_{PEO,\ DMAc}$ values were 1.14 and 9.21, respectively. However, because the GT equation can only be fitted to the upper and lower T_g values separately and there is no mixing of the DMAc with the PEO, the resulting $k_{PEO,\ DMAc}$ values should not be considered.

The T_g values for the PEO mass fractions of 5 %, 10 %, and 20 % samples show a decreasing trend from 55.4 °C, 53.8 °C, and 48.7 °C, respectively. As illustrated in Fig. 6, the three-component GT model, represented by the red-dashed line, does not align well with the data, while the Lodge-McLeish model, represented by the blue-dashed line, aligns well.

Deviations from the three-component GT equation are expected above mass fractions of 30 % PEO, where immiscibility begins. However, even within the miscibility range, the equation does not fully capture the T_g behavior, indicating that the blend T_g does not conform to the additive mass combination of the individual component T_g as the equation predicts. Instead, the blend's T_g is most likely influenced by other factors, such as hydrogen bonding, where PMMA is known to hydrogen bond with solvents, changing PMMA's thermal and mechanical properties [27]. Both the GT and Lodge-McLeish model capture the lower T_g values, yet are slightly different in their slopes.

3.4. Rheological response of the PEO:PMMA(DMAc) blends

The dynamic moduli, for the neat PMMA, PEO mass fraction of 0 %, neat PEO, and PEO mass fraction of 100 %, are presented in Figs. 7 and 8 as master curves created through frequency-temperature superposition. The data for the individual frequency scans are presented in the Supplemental Information. The figures include the data for the press-molded neat PMMA and the neat PEO, as well as that for the solvent-cast plaques at mass fraction of 0 % and 100 % PEO that were cast from the DMAc. These master curves highlight the differences between the neat polymers and their solvent-cast counterparts. For the neat PEO and 100:0 plaque (Fig. 7), no differences are observed as a result of the solvent-casting process, consistent with the comments above that mass loss in the PEO at higher temperatures is due to degradation. In contrast, a significant discrepancy is evident between the neat PMMA and the 0:100 plaque (Fig. 8). This disparity is attributed to the presence of the DMAc that remains in the PMMA following the solvent-casting process, as discussed earlier.

The dynamic moduli master curves created by frequency-temperature superposition for the different blended systems are shown in Fig. 9. The superposition was performed by shifting the tan(δ) curves (SI; Fig. S7) to acquire the horizontal shift factors independently from vertical shifts. Vertical shifting was applied as necessary to G' (and G″). The reference temperature was chosen to be the DSC determined T_g for each composition. Since the reference temperature was outside the range of temperatures studied, the Vogel-Fulcher-Tammann (VFT) equation was used to determine the shift factors. The relevant temperature was less than 5 °C from the experimental temperatures studied. The miscible samples, mass fractions of 5 %, 10 %, and 20 % PEO, and the immiscible sample, 30 % mass fraction of PEO, showed good superposability across all frequencies. The fact that the immiscible samples show good superposability is not unexpected, as the rheological tests were conducted above the melting point of PEO, 60.6 °C, where the samples are thought to be homogeneous [7,9,17,40]. However, the 30 % mass fraction of PEO sample also showed good superposability at the

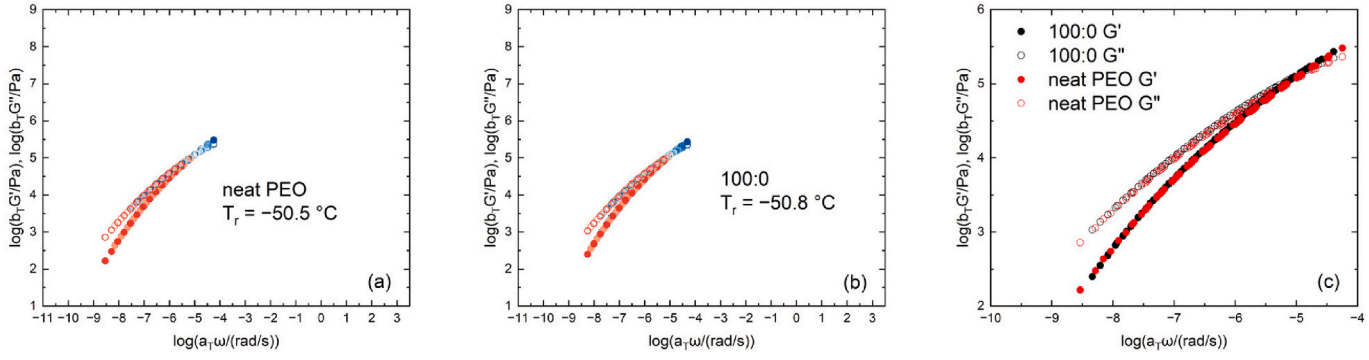

Fig. 7. Neat PEO (a) and 100:0 (b) master curves. The temperatures are 60 °C (●), 70 °C (●), 80 °C (●), 90 °C (●), 100 °C (●), 110 °C (●), and 120 °C (●). Comparison of the neat PEO and 100:0 plaque (c). Closed and open symbols represent G′ and G″, respectively. Here, a_T is the horizontal shift factor applied to the frequency to account for temperature effects on relaxation.

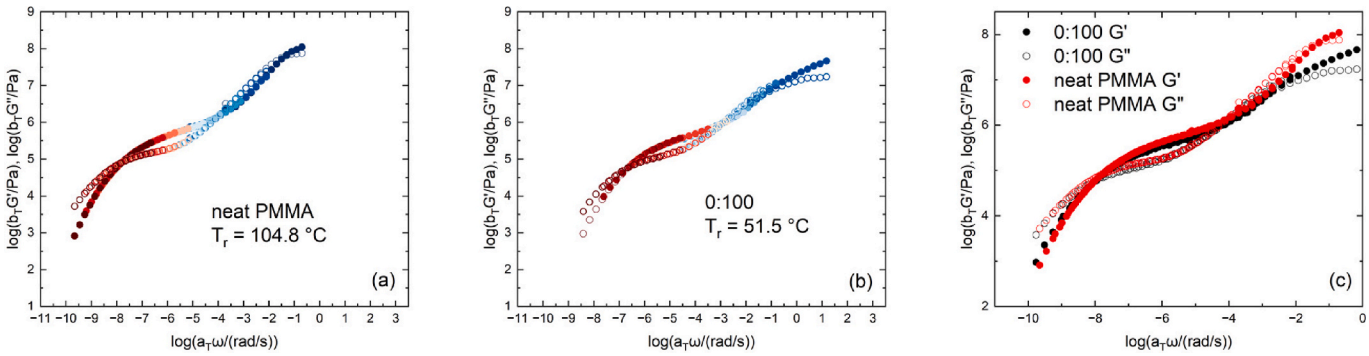

Fig. 8. Neat PMMA (a) and 0:100 (b) master curves. The temperatures are 120 °C (●), 130 °C (●), 140 °C (●), 150 °C (●), 160 °C (●), 170 °C (●), 180 °C (●), 190 °C (●), and 200 °C (●) for neat PMMA and 50 °C (●), 60 °C (●), 70 °C (●), 80 °C (●), 90 °C (●), 100 °C (●), 110 °C (●), 120 °C (●), 130 °C (●), and 140 °C (●) for 0:100. Comparison of the neat PMMA and 0:100 plaque (c). Closed and open symbols represent G′ and G″, respectively.

lowest temperature (50 °C), which is approximately 10 °C below the melting point of PEO. This could be attributed to solvent in the samples cast from DMAc, which affects the blend's relaxation behavior and increases mobility within the plaques. Another explanation may be that the blend did not have time to phase separate going from high to low temperatures during the rheological experiments.

To gain a deeper understanding of the behavior of the samples, we examined the temperature dependence of the shift factors used to create the master curves and depict log a_T *vs.* T in Fig. 10. The shift factors were fitted to the VFT equation,

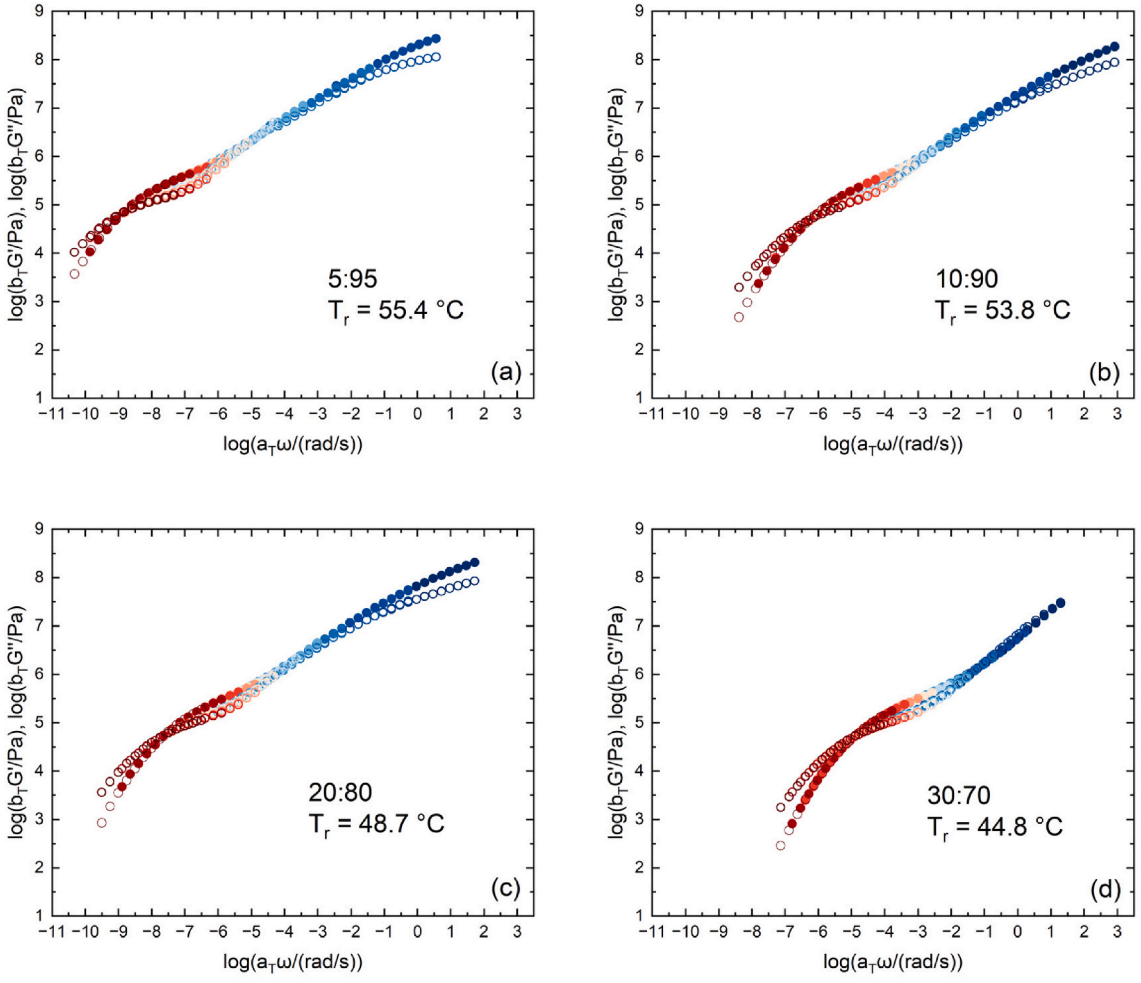

Fig. 9. Dynamic modulus master curves from frequency-temperature superposition for the solvent-cast PEO:PMMA(DMAc) blends 5:95 (a), 10:90 (b), 20:80 (c), and 30:70 (d). The temperatures are 50 °C (●), 60 °C (●), 70 °C (●), 80 °C (●), 90 °C (●), 100 °C (●), 110 °C (●), 120 °C (●), 130 °C (●), and 140 °C (●). Closed and open symbols represent G′ and G″, respectively.

$$a_T = Ae^{\frac{B}{(T-T_\infty)}} \quad (2)$$

where $a_T = \tau(T)/\tau_{T_g}$ is the horizontal shift factor, T is temperature, T_g is the glass transition temperature, τ is the relaxation time at T, τ_{T_g} is the relaxation time at T_g, and A, B and T_∞ are material-dependent constants. The VFT fit-determined parameters are presented in Table 2. For purposes of comparison, the reference temperatures were chosen to be the T_g of each sample as determined from DSC and are presented in Table 2.

From Table 2, we see that the VFT parameters are close to the "universal" VFT parameters obtained upon calculation from the "universal" William-Landel-Ferry (WLF) parameters and the relationship between the VFT and WLF equations [41]. The universal values of B and $(T_g - T_\infty)$ are approximately 2072 K and 51.6 K, respectively [42]. The 0:100 plaque is an outlier in that it shows a large difference in its VFT parameters from the universal values. This difference is likely attributed to the presence of DMAc and the possible overlap of the α- and β-relaxations of PMMA, as observed in the temperature sweeps in the previous section. Other contributing factors may include unknown interactions between DMAc and PMMA or the introduction of density fluctuations. The 0:100 sample is analyzed in greater detail in the following section using van-Gurp Palmen (vGP) plots.

Furthermore, the vertical shift factors (b_T) for the polymer blends and the 0:100 sample are unexpectedly large. While such magnitudes are atypical, they are considered allowable in thermorheological simplicity analysis according to the work from Markovitz [43]. These large vertical shifts may stem from DMAc induced density fluctuations or heterogeneities within the blends. However, the lack of a direct correlation with compositional changes casts doubts on the density fluctuations. Instead, the large vertical shift factors in the 0:100 sample suggest that DMAc is shifting the α- and β-relaxation of PMMA closer together, which has been shown in the previous section. At the same time, superposability with TTS works with such large vertical shift factors; however, the vGP plots do not superimpose as shown below, these plots seem to be more sensitive to the breakdown of TTS [4] than the "master" curves themselves. Before further examining the vGP plots, the dynamic fragility parameters of the blends are investigated.

The dynamic fragility m is a measure of the strength of the glass-formation process that was popularized by Angell [44] and it is of interest to examine the dependence of m on the blend composition. The value of m is related to the slope of the plot of the log of the dynamic variable (viscosity, relaxation time, shift factor) vs. T_g/T evaluated at $T = T_g$.

$$m = \frac{dlog(a_T)}{d\left(\frac{T_g}{T}\right)_{T=T_g}} \quad (3)$$

Materials are categorized into strong and fragile glass formers, where strong glass formers express close to Arrhenius behavior (close to straight line on the "Angell" plot), while fragile glass formers follow a strong VFT-type dependence on temperature (plots are strongly curved upwards). The fragility parameter, m, can be calculated from the VFT parameters using Equation (4) [45], where higher values are considered to represent a more fragile glass former.

$$m = \frac{BT_g}{\ln(10)(T_g - T_\infty)^2} \quad (4)$$

From Table 2, we see that neat PMMA expresses a higher fragility parameter than neat PEO, indicating that PMMA is a more fragile glass former. Incorporation of DMAc into PMMA lowers the fragility parameter relative to neat PMMA, although it still remains higher than that of neat PEO. Additionally, the fragility parameter decreases with increasing PEO content, from mass fractions of 5 % to 30 % PEO, suggesting that the blends exhibit stronger behavior with increasing PEO content. Notably, the 0:100 plaque showed a stronger glass forming behavior than PMMA(DMAc). Previous work [45] has reported a positive correlation between m and T_g, supporting this observation. Although, the correlation was based on a broad scattering of the reported data and the PMMA(DMAc) is an outlier within the trend.

3.5. Van Gurp-Palmen analysis of the rheological data

Van Gurp and Palmen [19] demonstrated that the validity of the TTS principle can be assessed by plotting the phase angle (δ) against the complex modulus ($|G^*|$). In this approach, when TTS holds, the data collected at different temperatures collapses onto a single curve without the need for shift factors. At low values of $|G^*|$, the curve begins in the terminal regime, where δ is at 90°. As the material transitions through the rubbery plateau, the curve reaches a minimum before rising again through the Rouse and sub-Rouse regimes, where a maximum is observed. Beyond this maximum, the curve approaches the glassy regime, where δ tends toward 0°. Moreover, Trinkle and Friedrich highlighted the sensitivity of vGP plots in characterizing the polydispersity of linear polymers [2], while Trinkle et al. have demonstrated their effectiveness in classifying long chain branched polymers [46]. Collectively, these insights emphasize how the vGP plot can be used as a

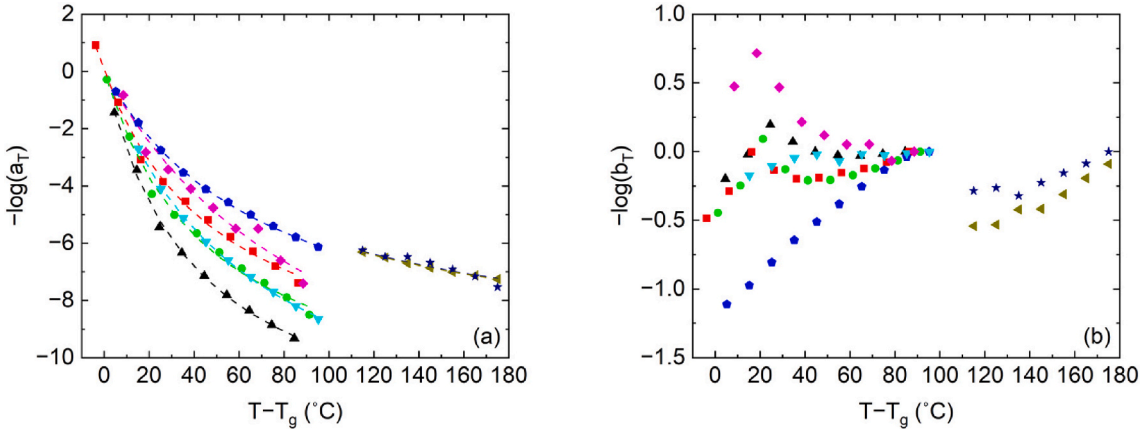

Fig. 10. Horizontal (a) and vertical (b) shift factors for the PEO:PMMA(DMAc) blends. PMMA (▼), 0:100 (◆), 5:95 (▲), 10:90 (■), 20:80 (●), 30:70 (⬟), 100:0 (◀), and PEO (★) plaques.

Table 2
VFT and fragility parameters for the PEO:PMMA(DMAc) blends.

PEO:PMMA(DMAc)	ln(A/Pa.s)	B (K)	T_∞ (K)	T_g (K)	m
Neat PMMA	−33.2 ± 1	2155 ± 230	313.1 ± 6	377.9 ± 0.3	84.1 ± 17
0:100	−34.9 ± 10	3580 ± 3200	222.0 ± 60	324.6 ± 1.6	47.9 ± 73
5:95	−32.9 ± 2	1588 ± 290	280.4 ± 7	328.6 ± 3.5	97.4 ± 36
10:90	−26.5 ± 2	1409 ± 280	273.8 ± 7	326.9 ± 1.2	70.8 ± 24
20:80	−28.8 ± 2	1364 ± 280	274.5 ± 8	321.9 ± 3.3	84.8 ± 34
30:70	−24.9 ± 1	1846 ± 170	243.9 ± 5	318.0 ± 3.8	46.5 ± 9
100:0	−23.2 ± 0.5	1524 ± 220	156.5 ± 15	222.4 ± 0.1	34.0 ± 16
Neat PEO	−23.1 ± 21	1524 ± 8600	156.5 ± 570	222.7 ± 0.3	33.7 ± 610

powerful tool for gaining a clearer understanding of material behavior.

Building on this framework, the vGP plots in Fig. 11 reveal a clear breakdown of TTS in the polymer blend plaques. The neat PMMA shows good superposability through the three regimes (terminal, Rouse, and glassy). In contrast, the 0:100, 5:95, 10:90, and 20:80 blends show good superposability in the terminal regime but a lack of superposition in the Rouse to glassy regime. The 30:70, 100:0, and neat PEO plaques show a lack of superposition throughout all the regimes. Interestingly, while neat PMMA exhibits favorable superposability, the solvent-cast PMMA plaque shows reduced superposability, suggesting that DMAc influences the vGP plots and leads to the large vertical shift factors seen in Table 2.

To further probe these deviations, the vGP plots were "corrected" by multiplying the complex modulus by the same vertical shift factors as those used in creating the time-temperature superposition master curves. By "correcting" the vGP plots with the vertical shift factors calculated by shifting G′, superposition should be expected since the master curves created by frequency-temperature superposition do not show obvious breakdown in the TTS principle. The vGP modulus "correction" does produce superposable behavior in the terminal regime; however, deviations persist near the Rouse to glassy regime as T_g is approached. This can be seen in Fig. 12. Here, the neat PMMA, neat PEO, 100:0, and 30:70 blends are superposable in all three regimes, while the 0:100, 5:95, 10:90, and 20:80 are superposable in the terminal regime and still fail to superpose in the Rouse to glassy regime. Notably, these deviations are not apparent in the TTS master curves but become evident in the vGP analysis, demonstrating the enhanced sensitivity of vGP plots for detecting subtle deviations from TTS.

The origin of this breakdown appears to be linked to the transition into the glassy state, where the temperature dependence of distinct relaxation times, potentially associated with spatial heterogeneities, becomes stronger and influences the dynamics near the glass transition temperature (T_g). These results suggest that, despite being previously described as miscible, the blends experience a breakdown in TTS and may not be fully compatible at the assumed compositions. An additional observation is the breakdown of superposability in the 0:100 plaque, even after vertical correction. While this effect is absent in the neat PMMA plaque near to T_g, it is clearly evident in the solvent-cast counterpart. Although both plaques show good superposability in their TTS master curves, the vGP plot for the 0:100 plaque demonstrates poor superposability near T_g.

This behavior may be attributed to DMAc influencing PMMA dynamics by causing the α- and β-relaxation to overlap. Other potential factors include density fluctuations. However, Chen et al. [47], investigated ring and linear polymer melts and solutions, observing that vGP plots become more superimposable with the addition of solvent, negating the influence of density or concentration fluctuations. While this is contrary to our observations and solvent-polymer interactions can differ, it suggests that DMAc may not be the sole contributor to the TTS breakdown. Other potential mechanisms for failure of TTS are discussed subsequently.

Given the sensitivity of vGP plots to subtle dynamic heterogeneities, it is important to examine how our results align with previous mechanistic interpretations of TTS failure. Haley and Lodge [48] considered the problem in terms of the self-concentration concept proposed by Lodge and McLeish [35] with a PEO (300 g/mol): PMMA (10,000 g/mol) blend and attributed the breakdown of TTS to the different temperature dependences of their terminal dynamics, i.e., PEO and PMMA have distinct temperature dependencies that lead to the breakdown of TTS. They also found that the terminal and segmental dynamics of PEO could not be directly correlated and had different temperature dependencies. However, in their study, like Colby's study, all rheological data were collected at high temperatures, well above the T_g of the blend. At this higher temperature, they reported a breakdown in TTS, while our study shows superposability in TTS, as well as in the more sensitive vGP plots. One issue for Haley and Lodge [48] is that their PEO was very low molecular weight and the PMMA was also an unentangled oligomer, thus the expected dynamics are not the same as those of terminal flow of an entangled system that one would see with the higher molecular weight polymers of this study and those of Colby [20] and of van Gurp and Palmen [19].

On the other hand, a breakdown of TTS is observed in the vGP plots in the present study as the temperature approaches the T_g. This phenomenon could be attributed to the increasing divergence in the temperature dependencies of the PEO and PMMA dynamics at lower temperatures [49]. While this explanation accounts for the behavior of polymer blends containing solvent, it does not describe the breakdown of TTS observed in the vGP plot for the 0:100 plaque. One possible explanation for the breakdown in the 0:100 plaque is that the solvent decreases the T_g, thereby reducing the temperature gap between the alpha and beta relaxations in PMMA. This reduced separation could allow the β-relaxation to disrupt the superposability of the curves, leading to the observed breakdown in TTS in the segmental relaxation regime. This idea is supported by the differences between the vGP plots of the neat PMMA and the PMMA(DMAc) systems (Fig. 11a and b and 12a,b). To investigate the possibility of spatial heterogeneity in the polymer blends being a cause of a breakdown of TTS approaching T_g, small-angle X-ray scattering was performed on the samples.

3.6. Results of X-Ray scattering from the blends

To further support the behavior seen in the rheological responses of the PEO:PMMA(DMAc) blends, we now discuss results from X-ray scattering experiments that provide insights into the spatial homogeneity and heterogeneity of several of the blends used in the rheological analysis. All of the scattering experiments were carried out at room temperature.

Fig. 13(a) presents the WAXS patterns for the neat polymers as well as the same series of blends with mass fractions of 100 %, 40 %, 30 %, 20 %, 10 % and 0 % PEO. The results indicate that neat PEO and the 100:0 are crystalline, whereas neat PMMA and the 0:100 plaque are amorphous. Additionally, the blends with 10 %, and 20 % PEO appear amorphous, while the blends with 30 %, and 40 % PEO exhibit slight crystallinity. The presence of crystallization peaks suggests that PEO has phase separated and crystallized within the blends. The WAXS results corroborate the DSC data in Fig. 6, as crystalline PEO diffraction peaks first appear in the 30 % PEO blend, confirming the samples with a mass fraction of 30 % PEO and above are immiscible below the melting point of PEO.

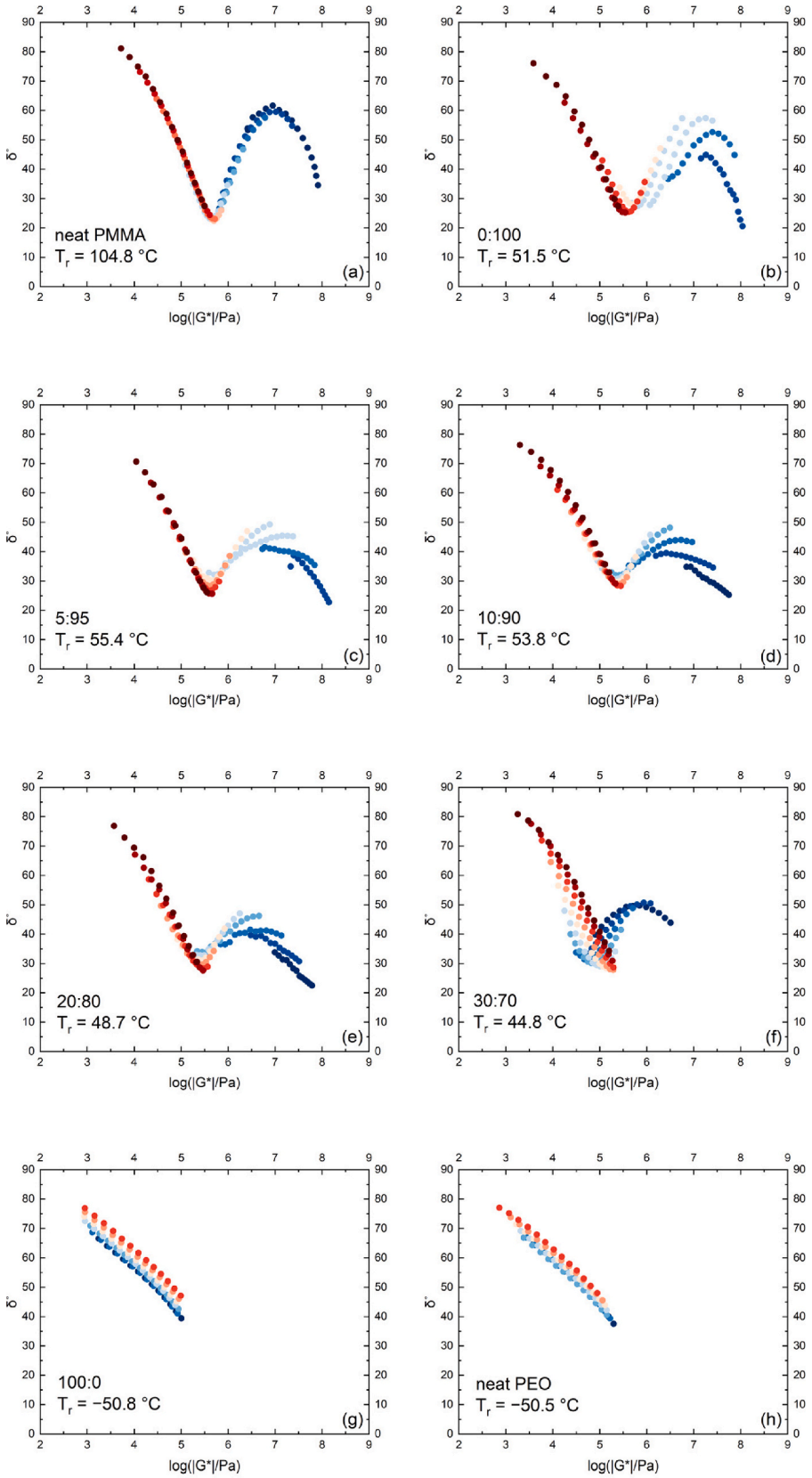

Fig. 11. vGP plots for the PMMA (a), 0:100 (b), 5:95 (c), 10:90 (d), 20:80 (e), 30:70 (f), 100:0 (g), and PEO (h) plaques. The temperatures are 50 °C (●), 60 °C (●), 70 °C (●), 80 °C (●), 90 °C (●), 100 °C (●), 110 °C (●), 120 °C (●), 130 °C (●), and 140 °C (●) except for PMMA that follows 120 °C (●), 130 °C (●), 140 °C (●), 150 °C (●), 160 °C (●), 170 °C (●), 180 °C (●), 190 °C (●), and 200 °C (●).

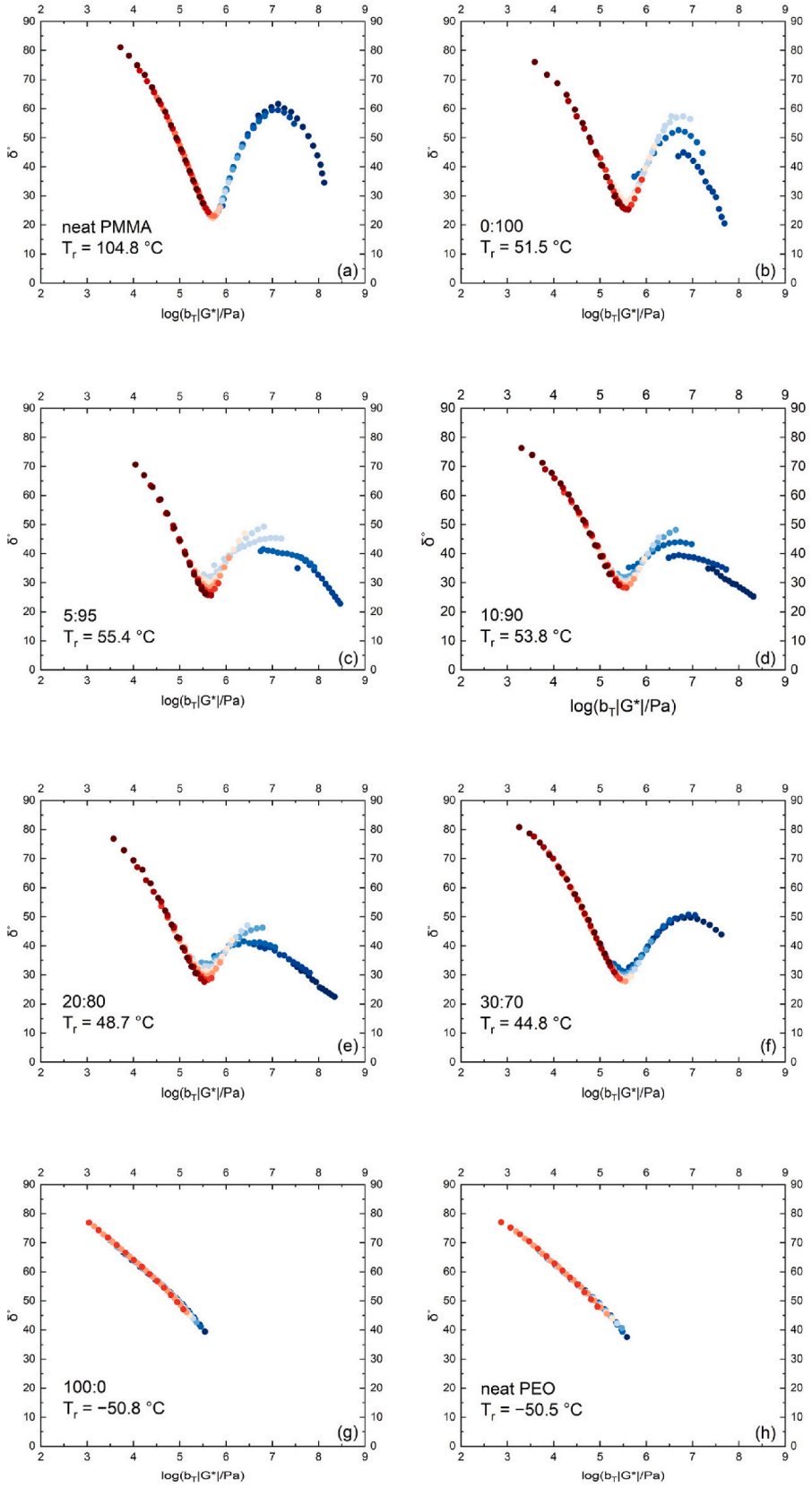

Fig. 12. Vertically (modulus shift factor b_T) corrected vGP plots for the PMMA (a), 0:100 (b), 5:95 (c), 10:90 (d), 20:80 (e), 30:70 (f), 100:0 (g), and PEO (h) plaques. The temperatures are 50 °C (●), 60 °C (●), 70 °C (●), 80 °C (●), 90 °C (●), 100 °C (●), 110 °C (●), 120 °C (●), 130 °C (●), and 140 °C (●) except for PMMA that follows 120 °C (●), 130 °C (●), 140 °C (●), 150 °C (●), 160 °C (●), 170 °C (●), 180 °C (●), 190 °C (●), and 200 °C (●).

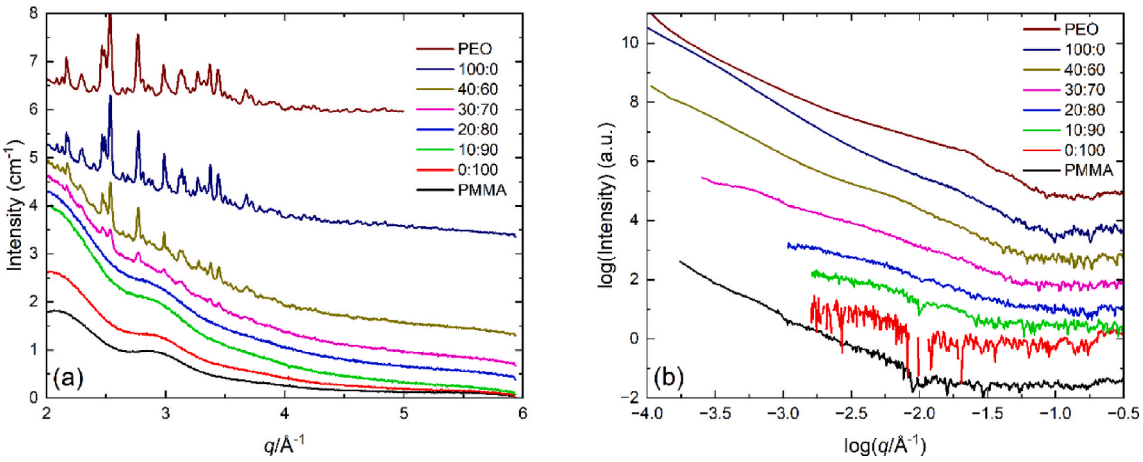

Fig. 13. WAXS patterns (a) and USAXS patterns (b) for the neat polymers and blends.

Fig. 13(b) presents the USAXS patterns for the same samples, while the corresponding SAXS patterns are provided in the SI. Comparing the SAXS patterns of neat PEO and the 100:0 plaque, the lamellar stacking for neat PEO is approximately 26 nm, whereas the 100 % PEO plaque shows a larger lamellar stacking of approximately 35 nm. This difference is not attributed to the solvent, as TGA and rheological data confirm its absence in the 100:0 plaque. Instead, the difference in lamellar stacking likely arises from differences in sample preparation: neat PEO was prepared by hot pressing PEO powder into a mold, while the 100:0 plaque was solvent cast from DMAc and not further treated. These different preparation methods influence the crystallization rates, leading to differences in lamellar size and potentially lamellar stacking [50].

Interestingly, despite the presence of crystallization in some blends as indicated by WAXS, lamellar stacking is not apparent in their SAXS patterns. Examination of the USAXS data in Fig. 13(b) shows that samples with higher PEO content exhibit increased scattering intensity and larger heterogeneities. To characterize the largest discernible length scales, we performed a Guinier analysis [51] of the low-q scattering. The resulting heterogeneity length scales for samples with mass fractions of 40 %, 30 %, 20 % and 10 % PEO are (443 ± 16) nm, (219 ± 6) nm, (65 ± 4) nm, and (25 ± 2) nm, respectively. This trend demonstrates that the largest discernible heterogeneity length scale increases with higher PEO content, and these values are substantially larger than the ~3 nm length scale typically associated with dynamic heterogeneity in glass-forming systems.

A particularly interesting observation is that the samples with mass fractions of 20 % and 10 % PEO, which were deemed miscible based on DSC and WAXS, have weak but discernible small-scale heterogeneities in the USAXS patterns. This provides a compelling explanation for the breakdown of TTS observed in the vGP plots near T_g. Although DSC and WAXS suggest miscibility, the USAXS data reveal heterogeneities at the 65 nm and 25 nm scale, aligning with the rheological observations of TTS breakdown. These small-scale heterogeneities, consisting of PEO and PMMA dominant phases, have different timescales that lead to the breakdown of TTS. Therefore, the dynamic heterogeneity observed at temperatures approaching T_g and below the melting point of PEO is most likely caused by these nanoscale spatial heterogeneities in the blend.

On another note, both the neat PMMA and 0:100 plaque show a similar Guinier turnover in the SAXS data at approximately 0.007 Å^{-1}, indicating comparable nanoscale structural features in the two samples. However, in the USAXS patterns, the neat PMMA follows a power-law slope in the low-q regime, which indicates a larger structure on the micrometer scale, while the 0:100 plaque does not. This is most likely due to the differences in the material processing. The addition of solvent in the 0:100 plaque results in decreased scattering intensity and a more uniform scattering length density compared to neat PMMA. This effect may be attributed to the solvent acting as a plasticizer, facilitating improved chain mobility and enhanced packing during solvent evaporation.

4. Conclusions

This study provides new insights into the interplay of spatial heterogeneity and dynamic behavior in PEO:PMMA blends, where the addition of DMAc modifies the PMMA phase, shifting its relaxation behavior closer to that of PEO. The resulting ternary PEO:PMMA(DMAc) blend shows excellent superposability under time-temperature superposition (TTS) in that one can readily create smooth master curves for both G′ and G″ by a combination of horizontal and vertical shifting, albeit with larger than generally observed vertical shifts for some of the systems. At the same time, we find that plotting the phase angle against the norm of the dynamic moduli (a van Gurp-Palmen representation) leads to the observation of non-superposability, hence highlighting the sensitivity of van Gurp-Palmen (vGP) analysis to subtle deviations from TTS. While the thermodynamic miscibility of PEO:PMMA blends has been well-documented, the present work provides a broader range of dynamics spanning from the terminal flow regime to near to the glassy or α-relaxation.

The lack of superposition in the vGP plot for the 0:100 sample is particularly interesting. The large vertical shift factors observed in the frequency-temperature superposition of the blends and the 0:100 sample suggest that DMAc is the primary driver of these shifts. While the shift factors are applied to both the vGP plots and the TTS master curves, the resulting breakdown in superposition is only apparent in the former. One explanation for this discrepancy is the shifting of the α- and β-relaxations causing them to overlap. This convergence could lead to a breakdown of superposition. Interestingly, there is no breakdown in the 30:70 sample in the master curve or vGP plot. Our results show that the PEO:PMMA(DMAc) blends show unique dynamic behavior, with superposition in the terminal regime and a breakdown in the glass regime. For the thermodynamically determined miscible blends, deviations in TTS, as seen by the vGP plots, suggest that small-scale heterogeneities persist even at compositions previously considered homogeneous when approaching the glass transition temperature. These results were further supported by the SAXS patterns that show 70 nm and 25 nm length scale heterogeneities in the previously considered miscible blends, at mass fractions of 20 % and 10 % PEO. Therefore, small-scale heterogeneities, with different temperature dependencies that are “stronger” near T_g, exist in the supposedly miscible blends. This observation is interesting given that the solvent shifted the glass transition temperature and relaxation processes of PMMA closer to those of PEO. One would expect that the blends would more easily be superimposable, given that the

solvent shifted the individual components' relaxation times closer together. However, this suggests that the dynamic processes for the PEO: PMMA(DMAc) ternary blend have different temperature dependences at temperatures below the rubbery regime but similar temperature dependences in the terminal regime. These differences become more pronounced when approaching T_g.

CRediT authorship contribution statement

Bret W. Tantorno: Conceptualization, Data curation, Formal analysis, Investigation, Methodology, Validation, Writing – original draft, Writing – review & editing. **Tuyen T.T. Truong:** Conceptualization, Investigation, Writing – original draft. **Lori M. Hoover:** Investigation. **Gregory B. McKenna:** Conceptualization, Funding acquisition, Investigation, Methodology, Project administration, Resources, Supervision, Writing – original draft, Writing – review & editing. **Ran Tao:** Investigation, Methodology, Writing – review & editing. **Fan Zhang:** Conceptualization, Formal analysis, Methodology, Writing – review & editing.

Declaration of competing interest

The authors declare that they have no known competing financial interests or personal relationships that could have appeared to influence the work reported in this paper.

Acknowledgements

We thank the American Chemical Society Petroleum Research Fund under grant 60750-ND7 andthe National Science Foundation under award 2219327 each for partial support of the project. This research used resources of the Advanced Photon Source, a U.S. Department of Energy (DOE) Office of Science User Facility operated for the DOE Office of Science by Argonne National Laboratory under Contract No. DE-AC02-06CH11357.

Appendix A. Supplementary data

Supplementary data to this article can be found online at https://doi.org/10.1016/j.polymer.2026.130287.

Data availability

Data will be made available on request.

References

[1] P.H.P. Macaúbas, N.R. Demarquette, Time-temperature superposition principle applicability for blends formed of immiscible polymers, Polym. Eng. Sci. 42 (7) (2002) 1509–1519, https://doi.org/10.1002/pen.11047.
[2] S. Trinkle, C. Friedrich, Van Gurp-Palmen-plot: a way to characterize polydispersity of linear polymers, Rheol. Acta 40 (4) (2001) 322–328, https://doi.org/10.1007/s003970000137.
[3] P. Reichert, B. Hoffmann, T. Bock, R. Thomann, R. Mülhaupt, C. Friedrich, Morphological stability of Poly(propylene) nanocomposites, Macromol. Rapid Commun. 22 (7) (2001) 519–523, https://doi.org/10.1002/1521-3927(20010401)22:7<519::AID-MARC519>3.0.CO;2-W.
[4] Z. Qian, G.B. McKenna, Expanding the application of the van Gurp-Palmen plot: new insights into polymer melt rheology, Polymer 155 (2018) 208–217, https://doi.org/10.1016/j.polymer.2018.09.036.
[5] B. Lu, K. Lamnawar, A. Maazouz, H. Zhang, Revealing the dynamic heterogeneity of PMMA/PVDF blends: from microscopic dynamics to macroscopic properties, Soft Matter 12 (13) (2016) 3252–3264, https://doi.org/10.1039/C5SM02659H.
[6] K. Assman, H.A. Schneider, The thermal analysis of polymer blends of poly (ethylene oxide)/poly(methyl methacrylate), J. Therm. Anal. 35 (2) (1989) 459–468, https://doi.org/10.1007/BF01904448.
[7] J. Baldrian, M. Horký, A. Sikora, M. Steinhart, P. Vlček, H. Amenitsch, S. Bernstorff, Time-resolved SAXS study of crystallization of poly(ethylene oxide)/poly(methyl methacrylate) blends, Polymer 40 (2) (1999) 439–445, https://doi.org/10.1016/S0032-3861(98)00246-8.
[8] S. Cimmino, E. Di Pace, E. Martuscelli, C. Silvestre, Evaluation of the equilibrium melting temperature and structure analysis of poly(ethylene oxide)/poly(methyl methacrylate) blends, Makromol. Chem. 191 (10) (1990) 2447–2454, https://doi.org/10.1002/macp.1990.021911022.
[9] C. Silvestre, S. Cimmino, E. Martuscelli, F.E. Karasz, W.J. MacKnight, Poly (ethylene oxide)/poly(methyl methacrylate) blends: influence of tacticity of poly (methyl methacrylate) on blend structure and miscibility, Polymer 28 (7) (1987) 1190–1199, https://doi.org/10.1016/0032-3861(87)90263-1.
[10] H. Ito, T.P. Russell, G.D. Wignall, Interactions in mixtures of poly(ethylene oxide) and poly(methyl methacrylate), Macromolecules 20 (9) (1987) 2213–2220, https://doi.org/10.1021/ma00175a028.
[11] Z. Bartczak, E. Martuscelli, Spherulites primary nucleation in binary miscible blends of poly(ethylene oxide) with poly(methyl methacrylate), Makromol. Chem. 188 (2) (1987) 445–453, https://doi.org/10.1002/macp.1987.021880220.
[12] C. Nakafuku, N. Toyonaga, Crystallization of poly(ethylene oxide) in a mixture with poly(methyl methacrylate) under high pressure, Polymer 33 (11) (1992) 2370–2375, https://doi.org/10.1016/0032-3861(92)90529-6.
[13] R. Pearce, G.J. Vancso, Observations of crystallization and melting in poly (ethylene oxide)/poly(methyl methacrylate) blends by hot-stage atomic-force microscopy, J. Polym. Sci. B Polym. Phys. 36 (14) (1998) 2643–2651, https://doi.org/10.1002/(SICI)1099-0488(199810)36:14<2643::AID-POLB17>3.0.CO;2-B.
[14] M. Dionísio, A.C. Fernandes, J.F. Mano, N.T. Correia, R.C. Sousa, Relaxation studies in PEO/PMMA blends, Macromolecules 33 (3) (2000) 1002–1011, https://doi.org/10.1021/ma9913818.
[15] A.C. Fernandes, J.W. Barlow, D.R. Paul, Blends containing polymers of epichlorohydrin and ethylene oxide. Part I: polymethacrylates, J. Appl. Polym. Sci. 32 (6) (1986) 5481–5508, https://doi.org/10.1002/app.1986.070320618.
[16] X. Li, S.L. Hsu, An analysis of the crystallization behavior of poly(ethylene oxide)/poly(methyl methacrylate) blends by spectroscopic and calorimetric techniques, J. Polym. Sci. Polym. Phys. Ed 22 (7) (1984) 1331–1342, https://doi.org/10.1002/pol.1984.180220715.
[17] S. Schantz, Structure and mobility in Poly(ethylene oxide)/Poly(methyl methacrylate) blends investigated by 13C solid-state NMR, Macromolecules 30 (5) (1997) 1 9–1425, https://doi.org/10.1021/ma961538l.
[18] J. Straka, P. Schmidt, J. Dybal, B. Schneider, J. Spěváček, Blends of poly(ethylene oxide)/poly(methyl methacrylate). An i.r. and n.m.r. study, Polymer 36 (6) (1995) 1147–1155, https://doi.org/10.1016/0032-3861(95)93916-A.
[19] M. van Gurp, J. Palmen, Time-temperature superposition for polymeric blends, Rheol.Bull. 67 (1998) 5–8.
[20] R.H. Colby, Breakdown of time-temperature superposition in miscible polymer blends, Polymer 30 (7) (1989) 1275–1278, https://doi.org/10.1016/0032-3861(89)90048-7.
[21] J.A. Zawada, C.M. Ylitalo, G.G. Fuller, R.H. Colby, T.E. Long, Component relaxation dynamics in a miscible polymer blend: poly(ethylene oxide)/poly (methyl methacrylate), Macromolecules 25 (11) (1992) 2896–2902, https://doi.org/10.1021/ma00037a017.
[22] P. He, W. Shen, W. Yu, C. Zhou, Mesophase separation and rheology of Olefin multiblock copolymers, Macromolecules 47 (2) (Jan. 2014) 807–820, https://doi.org/10.1021/ma402330a.
[23] S.A. Hutcheson, G.B. McKenna, The measurement of mechanical properties of glycerol, m-toluidine, and sucrose benzoate under consideration of corrected rheometer compliance: an in-depth study and review, J. Chem. Phys. 129 (7) (2008) 074502, https://doi.org/10.1063/1.2965528.
[24] K. Schröter, S.A. Hutcheson, X. Shi, A. Mandanici, G.B. McKenna, Dynamic shear modulus of glycerol: corrections due to instrument compliance, J. Chem. Phys. 125 (21) (2006) 214507, https://doi.org/10.1063/1.2400862.
[25] C.T. Moynihan, A.J. Easteal, M.A. De Bolt, J. Tucker, Dependence of the fictive temperature of glass on cooling rate, J. Am. Ceram. Soc. 59 (1–2) (1976) 12–16, https://doi.org/10.1111/j.1151-2916.1976.
[26] J. Ilavsky, et al., Development of combined microstructure and structure characterization facility for in situ and operando studies at the Advanced Photon Source, J. Appl. Crystallogr. 51 (3) (2018) 867–882, https://doi.org/10.1107/S160057671800643X.
[27] N. Patra, A.C. Barone, M. Salerno, Solvent effects on the thermal and mechanical properties of poly(methyl methacrylate) casted from concentrated solutions, Adv. Polym. Technol. 30 (1) (2011) 12–20, https://doi.org/10.1002/adv.20203.
[28] J.D. Ferry, Viscoelastic Properties of Polymers, third ed., John Wiley & Sons, New York Chichester Brisbane Toronto Singapore, 1980, p. 283.
[29] Data from NIST Standard Reference Database 69: NIST Chemistry WebBook. http://webbook.nist.gov/chemistry/. (Accessed 25 October 2024).
[30] X. Peng, J.G. Wang, Q. Li, D. Chen, R.N. Zia, G.B. McKenna, Exploring the validity of time-concentration superposition in glassy colloids: experiments and simulations, Phys. Rev. E 98 (6) (2018) 062602, https://doi.org/10.1103/PhysRevE.98.062602.
[31] R. Zorn, G.B. McKenna, L. Willner, D. Richter, Rheological investigation of polybutadienes having different microstructures over a large temperature range, Macromolecules 28 (25) (1995) 8552–8562, https://doi.org/10.1021/ma00129a014.
[32] M.L. Cerrada, G.B. McKenna, Physical aging of amorphous PEN: isothermal, isochronal and isostructural results, Macromolecules 33 (8) (2000) 3065–3076, https://doi.org/10.1021/ma990400a.
[33] N.S. Vrandečić, M. Erceg, M. Jakić, I. Klarić, Kinetic analysis of thermal degradation of poly(ethylene glycol) and poly(ethylene oxide)s of different molecular weight, Thermochim. Acta 498 (1) (2010) 71–80, https://doi.org/10.1016/j.tca.2009.10.005.
[34] T.P. Lodge, E.R. Wood, J.C. Haley, Two calorimetric glass transitions do not necessarily indicate immiscibility: the case of PEO/PMMA, J. Polym. Sci. B Polym. Phys. 44 (4) (2006) 756–763, https://doi.org/10.1002/polb.20735.

[35] T.P. Lodge, T.C.B. McLeish, Self-Concentrations and effective glass transition temperatures in polymer blends, Macromolecules 33 (14) (2000) 5278–5284, https://doi.org/10.1021/ma9921706.
[36] W. Zheng, S.L. Simon, The glass transition in athermal poly(α-methyl styrene)/oligomer blends, J. Polym. Sci. B Polym. Phys. 46 (4) (2008) 418–430, https://doi.org/10.1002/polb.21379.
[37] M. Gordon, J.S. Taylor, Ideal copolymers and the second-order transitions of synthetic rubbers. i. Non-crystalline copolymers†, J. Appl. Chem. 2 (1952) 493–500, https://doi.org/10.1002/jctb.5010020901.
[38] Walter Kauzmann, The Nature of the glassy State and the behavior of liquids at low temperatures, Chem. Rev. 43 (2) (1948) 219–256, https://doi.org/10.1021/cr60135a002.
[39] R.G. Beaman, Relation between (apparent) second-order transition temperature and melting point, J. Polym. Sci. 9 (5) (1952) 470–472, https://doi.org/10.1002/pol.1952.120090510.
[40] M.M. Cortazar, M.E. Calahorra, G.M. Guzmán, Melting point depression in poly (ethylene oxide)-poly (methyl methacrylate) blends, Eur. Polym. J. 18 (2) (1982) 165–166, https://doi.org/10.1016/0014-3057(82)90196-3.
[41] J.D. Ferry, Viscoelastic Properties of Polymers, third ed., John Wiley & Sons, New York Chichester Brisbane Toronto Singapore, 1980.
[42] J. Dudowicz, J.F. Douglas, K.F. Freed, The meaning of the 'universal' WLF parameters of glass-forming polymer liquids, J. Chem. Phys. 142 (1) (2015) 014905, https://doi.org/10.1063/1.4905216.
[43] H. Markovitz, Superposition in rheology, J. Polym. Sci.: Polymer Symposia 50 (1) (1975) 431–456, https://doi.org/10.1002/polc.5070500122.
[44] C.A. Angell, Spectroscopy simulation and scattering, and the medium range order problem in glass, J. Non-Cryst. Solids 73 (1) (1985) 1–17, https://doi.org/10.1016/0022-3093(85)90334-5.
[45] Q. Qin, G.B. McKenna, Correlation between dynamic fragility and glass transition temperature for different classes of glass forming liquids, J. Non-Cryst. Solids 352 (28) (2006) 2977–2985, https://doi.org/10.1016/j.jnoncrysol.2006.04.014.
[46] S. Trinkle, P. Walter, C. Friedrich, Van Gurp-Palmen Plot II – classification of long chain branched polymers by their topology, Rheol. Acta 41 (1) (2002) 103–113, https://doi.org/10.1007/s003970200010.
[47] D. Chen, et al., Linear viscoelastic properties of putative cyclic polymers synthesized by reversible radical recombination polymerization (R3P), Macromolecules 56 (3) (Feb. 2023) 1013–1032, https://doi.org/10.1021/acs.macromol.2c00892.
[48] J.C. Haley, T.P. Lodge, Dynamics of a poly(ethylene oxide) tracer in a poly(methyl methacrylate) matrix: remarkable decoupling of local and global motions, J. Chem. Phys. 122 (23) (2005) 234914, https://doi.org/10.1063/1.1931656.
[49] M. Brodeck, F. Alvarez, A.J. Moreno, J. Colmenero, D. Richter, Chain motion in Nonentangled dynamically asymmetric polymer blends: Comparison between atomistic simulations of PEO/PMMA and a generic bead−spring model, Macromolecules 43 (6) (2010) 3036–3051, https://doi.org/10.1021/ma902820a.
[50] B. Lee, et al., Time-resolved X-ray scattering and calorimetric studies on the crystallization behaviors of poly(ethylene terephthalate) (PET) and its copolymers containing isophthalate units, Polymer 44 (8) (2003) 2509–2518, https://doi.org/10.1016/S0032-3861(03)00130-7.
[51] Small angle scattering of X-rays, A. Guinier, G. Fournet, in: K.L. Yudowitch (Ed.), Translated by C. B. Wilson and with a Bibliographical Appendix, Wiley, New York, 1955, p. 268. $7.50.